Theory of Coupled-Mode Self-Excited Vibration of Tainter Gates

K.Sarth Chandra[1] C.Chandramohan[2] Ayub Ashwak[3]
[1]*Professor, Department of Mechanical, Faculty of HITS ,Hyderabad ,India.*
[2]*Professor, Department of Mechanical, Faculty of HITS, Hyderabad,India.*
[3]*Asso. Professor, Department of Mechanical, Faculty of HITS, Hyderabad India.*

Abstract:-The theoretical analysis of coupled-mode self-excited vibration of hydraulic gates is developed in the present paper. The theory is applied to the 87-ton Tainter gate at the Folsom Dam, which according to eyewitness testimony, experienced flow-induced vibrations and failed in l995. In its original design, the Folsom Tainter gate possessed two significant vibration modes. One mode was a whole gate rotation around the trunnion pin, while the second mode was a streamwise bending vibration of the skinplate. For certain upstream water levels, these two modes can couple with each other through hydrodynamic forces and inertia torques, producing self-excited vibration. The equations of motion for the small amplitude coupled-mode vibration are derived in non-dimensional form, revealing the non-dimensional parameters governing the vibrations and the hydrodynamic forces. The characteristics of this coupled-mode self-excited vibration are obtained through approximate numerical solutions, derived by iterative numerical calculations of the equations of motion. In addition, examination and physical explanations for vibration trajectories and energy transfer from the fluid motion to the gate vibration are presented. The theory, along with measured in-air frequencies, mode shapes and damping ratios, is used to generate stability diagrams of the original Folsom gate design.
Keywords:- Vibration, Flow-induced, Tainter gate, Coupled-mode, Self-excited, Equations of motion

I. INTRODUCTION

Tainter gates (also known as radial gates) are used frequently as crest gates on dam spillways for water level regulation. The design of these Tainter gates is such that the resultanthydraulic load due to pressure exerted on the skinplate usually passes through the trunnion pin. In this manner, the hydraulic load is usually borne by the trunnion pin as shown in Figure 1. The effect of mechanical friction in Tainter gates is much less than in the other type of gate, such as vertical lift gates, and a portion of the gate weight is also carried by the trunnion pin, permitting the use of a relatively a small capacity hoisting motor and smooth operation of the gate. For this reason, Tainter gates are well suited for larger installations.

Figure 1: Side View of the 87-ton Tainter Gate from the Folsom Dam in California, Showing Two Predominant Natural Vibration Modes

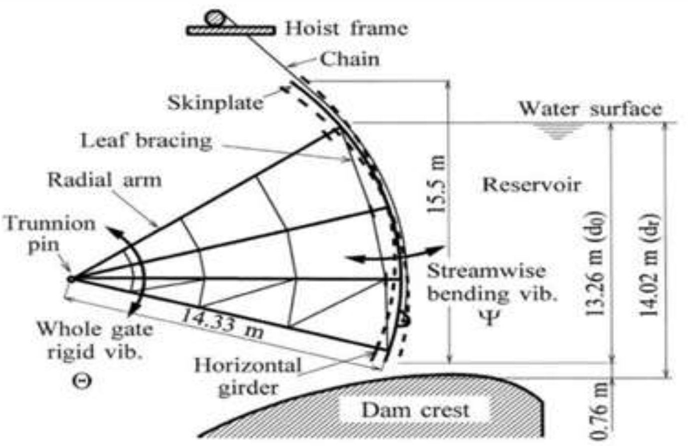

A drawing of a Tainter gate, previously installed at the Folsom Dam on the American River near Sacramento, California is shown in Figure 1. The gate has a height of 15.5 m, a width of 12.8 m and the curved skinplate radius of 14.33 m. The whole gate mass is 87.03×10^3 kg. According to an eyewitness account, one of these massive Tainter gates experienced flow-induced vibrations and failed, early in the morning of July 17, 1995. The gate operator was on the catwalk just above the gate to opening the gate. He said
he felt a small steady vibration starting up, initially very light, but then quickly intensifying. Upon his initial observation, the operator pushed the stop button, thinking to close the gate. As he turned from the control panel,

he saw the one side of the gate moving slowly in the downstream direction, rotating about the other side of the gate, like a large hinged garage door, as detailed by Ishii (1995a).

In an earlier case, a Tainter gate, with a height of 12 m, a width of 9 m, a radius of 13 m and a mass of 37×10^3 kg at the Wachi Dam in Japan failed and was swept downstream about 140 m on July 2, 1967 (Ishii *et al.*, 1980). More than 30 years ago, the review team for this gate failure in Japan suggested that flow-induced vibrations as a possible cause. However, at that time there was no known vibration mechanism and the structural dynamics of such large gates had not been well studied.

In examining the Wachi Dam gate failure, a dangerous type of flow-induced vibration of radial gates resulting from the eccentricity of the curved skinplate center relative to the trunnion center was identified. This “eccentricity instability” was first suggested by Imaichi and Ishii (1977), and subsequently studied by Ishii and Imaichi (1977), Ishii *et al.* (1977) and Ishii *et al.* (1979), as well as by Ishii and Naudascher (1992). A careful examination of the Wachi gate drawing revealed that the gate eccentricity was only 72 mm, and this small eccentricity was later shown to be insufficient to excite the eccentricity vibration mechanism. Ishii (1995a) had an initial suspicion that this “eccentricity instability” may have played a role in the Folsom Dam failure.

For the onset of this eccentricity self-excited vibration, however, the skinplate center eccentricity from the trunnion pin center would have had to have been more than 0.42 m for the Folsom gate. The radial gate at the Folsom Dam did not possess such an eccentricity between the skinplate center and trunnion center. The Folsom Dam failure then strongly suggests a “non-eccentricity hydrodynamic instability” to which Tainter gates with no skinplate eccentricity may be susceptible. In a companion paper, Anami *et al.* (2014) reviewed the structural dynamics of the original Folsom Dam gate, and presented FEM results that suggests the static loading was insufficient, by itself, to cause the gate failure. In the companion paper, the authors developed a conceptual model of a coupled-mode self-excited hydrodynamic instability, resulting from the coupling of two modes of vibration through inertia forces and hydrodynamic forces on the gate.

As a first step in the exploration of a potential vibration mechanism for the Folsom Dam gates, in late September 1995, Ishii (1995b) conducted in-air experimental modal analysis tests on one of the remaining geometrically similar Folsom Dam gates (subsequently designated as the “original gate”), employing an impact hammer and accelerometers. From these modal analysis tests, a relatively precise assessment of the natural vibration characteristics of the failed gate was obtained. After this initial modal analysis, the remaining gates were reinforced. Subsequently, in the middle of November 1996, similar experimental modal analysis tests were conducted on one of the reinforced Folsom Dam gates in order to evaluate the dynamic effectiveness of the reinforcement (see Ishii, 1997 for details). The experimental modal analyses, presented in detail in Anami *et al.* (2014), identified two significant vibration modes. One mode was the whole gate rotation around the trunnion pin with a frequency of 6.88 Hz. The other mode was a streamwise bending vibration of the skinplate, associated with the deformation of the radial arm structures, with a in-air frequency of 26.9 Hz, characterized by predominantly streamwise bending of the skinplate about a horizontal nodal line corresponding to the location of the second horizontal girder, as illustrated in Figure 2.

The whole gate rotation induces a “flow-rate variation pressure” introduced by Ishii (1992) and a coupled inertia torque on the skinplate, both of which excite the skinplate to rotate in the streamwise direction. Subsequently, the skinplate streamwise rotation induces another large hydrodynamic force producing a significant added mass effect, and the inertia torque is fed back to excite the whole gate rotation. The pressure loading, corresponding to the large hydrodynamic force producing the added mass effect, has been called the “push-and-draw pressure” by Anami and Ishii (1998a).

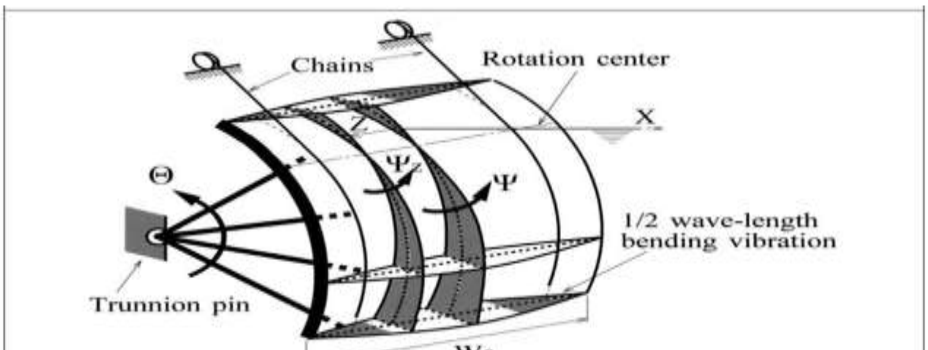

Figure 2: Schematic View of Tainter Gate Low Frequency Skinplate Bending Mode in the Streamwise Vertical Direction, and 1/2 Wave-Length Mode in the Spanwise Direction

With the gate motion in each mode generating a driving force for the other mode, the two vibration modes couple very effectively with each other through the hydrodynamic forces and inertia torques, resulting in a violent coupled-mode self-excited vibration under certain conditions. It is emphasized that this mechanism may potentially excite any Tainter gate, even those with zero eccentricity between the trunnion center and the skinplate center.

Theoretical analysis of this potentially disastrous coupled-mode self-excited vibration requires the calculation of the push-and-draw pressure induced by a streamwise rotation of the skinplate. The methodology for this calculation was introduced by Anami and Ishii (1998a). It was later carried out specifically for the Folsom gate by Anami *et al.* (2012a). Subsequently, the theoretical development requires a method to calculate the in-water natural vibration frequency of the skinplate rotation. Such a method was documented in Anami and Ishii (1998b). In a later publication, Anami *et al.* (2012b) provide the calculation of the in-water natural frequency for the skinplate of the Folsom Dam. Based on the measured in-air natural frequency of 26.9 Hz, Anami *et al.* (2012b) find the in-water natural vibration frequency of the skinplate ending mode for the Folsom Dam gate to be 6.46 Hz under the conditions at the time of failure. The significant reduction in the bending mode frequency stems directly from the huge added mass effect, and produces a relatively tight frequency coherence between the skinplate bending mode and the whole gate rotational vibration around the trunnion pin at a frequency of 6.88 Hz.

In this study, previously developed expressions for push-and-draw pressure and flow-rate-variation pressure are applied to the coupled-mode vibration of the Folsom Dam Tainter gate to derive the equations of motion assuming small amplitudes. The equations of motion are reduced to a non-dimensional form. The non-dimensional equations provide guidance on the appropriate non-dimensional parameters, such as a reduced added mass, reduced fluid damping and excitation coefficients for hydrodynamic forces, as well as the water-to-gate mass ratio and the moment-of-inertia ratio for vibrations. Ultimately, based on the derived equations of motion, a closed energy cycleis presented, which predicts the susceptibility of the Folsom Dam Tainter gate to the coupled-mode self-excited instability under the conditions prevailing at the time of failure.

II. EQUATIONS OF MOTION

Coupled Torque of Inertia

Figure 2 provides a three-dimensional illustration of the skinplate bending vibration. In the streamwise vertical plane, the skinplate exhibits a low-frequency bending mode, essentially performing a rotational vibration around a horizontal nodal line, termed the "streamwise-rotation center line." The counter-clockwise rotation of the skinplate along the spanwise center line, as shown in Figure 2 with the upstream reservoir to the right, is represented by θ. In the spanwise horizontal plane, the skinplate exhibits a half-wave-length bending mode shape with nodes at each end. Therefore, θ_z, the rotational angle of the skinplate at a given spanwise distance Z from the spanwise center, can be approximated by

$$\theta_z = \theta \sin\{\pi (Z/W_0 + 1/2)\} \qquad ...(1)$$

where W_0 is the spanwise length of the skinplate, as shown in Figure 2.

A schematic view of the skinplate element with a small spanwise length of dZ is shown in Figure 3, where the element performs a rotation around the trunnion pin, represented by ϕ, in addition to the streamwise counter-clockwise-rotation represented by θ_z, with a counter clockwise rotation defined as positive.

These two rotational vibrations can very effectively couple with each other through the inertia forces on the skinplate, that is, through the so-called "coupled inertia torque." The coupled inertia torque around the skinplate rotation center due to the whole gate rotational vibration around the trunnion pin is represented by $dM_{\theta\phi}$, while the coupled inertia torque around the trunnion pin due to the skinplate streamwise rotational vibration is denoted by $dM_{\phi\theta}$. Each differential coupled inertia torque can be obtained by integrating the moment due to the inertia forces on the infinitesimal skinplate element.

A small cross-section of the skinplate is indicated by the small black differential element in Figure 3. The mass of this differential element per the unit span is denoted by dm and the mass for the differential element with span *dZ* is *dmdZ*. Multiplying the mass by the tangential accelerations $R_{□}$ □ and $R_{□}$ $□_z$ yields the tangential inertia forces (–*dmdZ* $R_{□}$ □) and (–*dmdZ* $R_{□}$ $□_z$), which are shown as vectors in Figure 3. Here, $R_{□}$ and $R_{□}$ represent the radii of rotation for each vibration, that is,

the distance from the trunnion pin and from the skinplate rotation center to the skinplate differential element, respectively. The present analysis assumes small vibrations, and hence the centrifugal forces can be neglected as second order relative to the tangential forces.

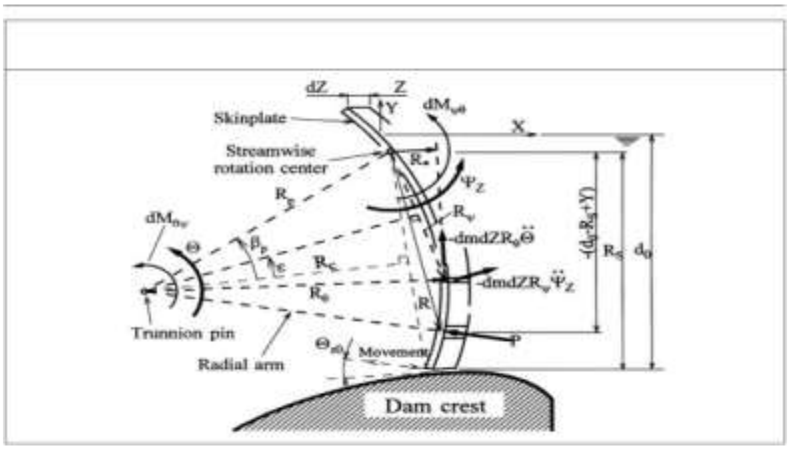

Each differential tangential inertia force by the moment arm to the center of rotation for the complementary vibration and then integrating each differential tangential inertial moment over the whole skinplate with a spanwise length *dZ* yields the streamwise and up-and-down coupled inertia torques $dM_{□□}$ and $dM_{□□}$ given by the following expressions:

$$dM_{□□} □ □ □_m □ dmdZ\, R_{□} □ R* \quad \text{or} \quad dM_{□□} □ □ □ \frac{I_{□}}{W_0} □ \, dZ \qquad ...(2)$$

$$dM_{□□} □ □_m □ dmdZ\, R_{□} □_z \frac{2}{R_{□}} \quad \text{or}$$

The tangential inertia force due to the □ vibration has an arm length of *R** from the skinplate rotation center, while the tangential inertia force due to the □ vibration has an arm length of $R_{□}$ /2 from the trunnion pin. Multiplying

$$dM_{□□} □ □ □ \frac{I_{□}}{2W_0} □_z \, dZ \qquad ...(3)$$

The subscript “*m*”on the integral represents integration over the spanwise-unit-length of the skinplate. $I_{□□}$ and $I_{□}$ are the moments of inertia of the whole skinplate, defined respectively by

I□ □ □ $^W 0$ □$_m$ ^{R}□ ^{R}∗dm ...(4)

I□ □ $^W 0$ □$_m$ ^{R}□ $^2 dm$ ...(5)

$I_{□□}$ represents the inertia effect on the skinplate streamwise vibration due to the whole gate vibration around the trunnion pin, while $I_{□}$ represents the inertia effect on the whole gate vibration around the trunnion pin due to the skinplate streamwise vibration. Together these two terms are called the "coupled moments-of-inertia" for the skinplate.

Basic Equations of Motion

The circular-arc skinplate center is assumed to coincide precisely with the trunnion pin, and hence the hydrodynamic pressure indicated by *P* in Figure 3 passes exactly through the trunnion pin center. Therefore, the hydrodynamic pressure cannot appear directly in the equation of motion of the whole gate rotational vibration around the trunnion pin. The whole gate is accelerated by the coupled inertia torque which can be obtained by integrating $dM_{□□}$ over the whole spanwise length, thus resulting in following equation of motion:

I□ □□□□□□ 2□ a□ □a□ □□□□□a□ □□□ □$_Z$ 2 $dM_{□□}$ □ 0 ...(6)

where $I_{□}$ is the moment of inertia of the whole gate around the trunnion pin, $□_{a□}$ and $z_{a□}$ are the in-air circular frequency and in-air damping ratio of the whole gate rotational vibration, respectively. The subscript "*Z*" on the integral represents integration over the spanwise length. Using Equations (1) and (3), the integration on *Z* leads to the following:

$dM_{□□}$ □□□ $I_{□}$ / $2W_0$ □ $W_0/2$ □ □ $sin_{□}$ □ □W $_0/2$ □ Z / □ $^W 0$ 2 □ $\underline{1}$ □ □□ □dZ □$_z$

I□ / $2W_0$ □ □ □ $\underline{2W_0}$ □ $I_{□}$ / □ □ □ □ □ □ ...(7)

$2W_0$ □ □

With this value for the integral, Equation (6) for the rigid-body motion of the whole gate around the trunnion pin can be arranged in the following form:

□□□ 2 □$_{a□}$□ $_{a□}$ 21 $I_{□}$ □□□□□$_{a□}$□□□ □ $I_{□}$ □□□0 ...(8)

In contrast to its role in the excitation of the whole gate rigid-body vibration, the hydrodynamic pressure *P* directly participates in the streamwise rotational vibration of the skinplate. The skinplate streamwise rotational vibration is excited by both the hydrodynamic force and the coupled inertia torque $dM_{□□}$, and thus has the following equation of motion:

□ □$_z$ □ 2□ $_{a□}$ □$_{a□}$ □$_z$ □ □ □$^2_{a□}$ □$_z$ □dZ

□$\underline{W}$ ^{0} $dM_{□□}$ □$\underline{W}$ $\underline{0}$ □$_R$$PR$ dR □ dZ □ 0 ...(9)

$I_{\square}$ $I_{\square}$

R represents the chord length from the skinplate rotation center to the pressure P. Integrating Equation (9) over the spanwise length, the equation of motion of the whole skinplate is given by:

$$\square_Z \square \square_z \square 2\square_{a\square} \square_{a\square} \square_z \square \square \square^2_{a\square} \square_z \square dZ$$

$$\square \, W_{I\square}^{0} \square_Z \frac{dM}{} \square \square \, W_{I\square}^{0} \square_Z \square_R PR\, dR \square dZ \square 0 \quad ...(10)$$

As shown in Figure 2, if the skinplate vibrates in the spanwise half-wavelength bending mode with a node of each side of the skinplate, the vibration-induced hydrodynamic pressure is naturally influenced by the half-wavelength bending vibration. Therefore, the integration with respect to Z can be carried out for all terms except for the hydrodynamic pressure term, resulting in the following expression:

$$\square \square \square 2\square_{a\square} \square_{a\square} \square \square \square \square^2_{a\square} \square$$

$$\frac{\square}{I\square \square} \square W_0 / 2$$

[redacted]

$$\square \square \square \square W_0$$

$$\square 2 I_{\square} \square 2I_{\square} / 2 \quad dZ \square_R PR\, dR \square 0 \quad ...(11)$$

where Equation (2) was substituted into Equation (10). $\square_{a\square}$ and $\square_{a\square}$ represent the in-air circular frequency and in-air damping ratio of the skinplate streamwise natural vibration, respectively.

Hydrodynamic Pressure

When the whole gate performs rotation around the trunnion pin, the flow-rate beneath the gate varies, producing the "flow-rate variation pressure", $P_{r\square}$. When the circular-arc skinplate performs streamwise rotational vibrations, the upstream water is pushed and drawn by the streamwise movement of the boundary, thus producing the "push-and-draw pressure", $P_{b\square}$. If the movement of the lower edge of the skinplate is not in the tangential direction of the dam crest curve, as shown in Figure 3, an additional flow-rate variation is induced by the streamwise rotation of the skinplate, producing the "additional flow-rate-variation-pressure", $P_{r\square}$. On these pressure terms, the subscripts "*r*" and "*b*" represent the flow-rate variation under the gate and the flow-boundary movement due to skinplate vibration, respectively. The second subscripts, "□ " and "□", represent the upward rotation of the whole gate and the streamwise rotation of the skinplate, respectively. Assuming amplitude vibrations for both of the skinplate streamwise rotational vibration and whole gate rotational vibration around the trunnion pin, and using the superposition principle, the resultant hydrodynamic pressure fluctuation P due to both vibrations occurring simultaneously is given by the summation of these pressure components:

$$P = P_{b\square} + P_{r\square} + P_{r\square} \quad ...(12)$$

Since the vibration amplitude in the half-wavelength mode is far smaller than the spanwise length of the skinplate, it is assumed here that the hydrodynamic pressure components are simply proportional to the streamwise and tangential vibration amplitudes of the lower-end of the skinplate. Each pressure component was analyzed, by applying the potential theory developed by Rayleigh (1945) for dissipative-wave radiation problems (Ishii, 1992; and Anami *et al.*, 2012b). The potential theory yields values of pressure fluctuations that agree well with experimental results (Anami *et al.*, 2012b). The three hydrodynamic pressure components can, therefore, be reduced to the following expressions:

$$p_{b\square} \square \frac{P_{b\square} / \square g}{R_s \square_0 \sin (Z / W_0 \square 1/2) \square} \quad ...(13a)$$

$$p_{r\square} \square \frac{P_{r\square} / \square g}{2\, c_f R_c \square_0} \quad ...(13b)$$

$$p_{r\square} \square \frac{P_{r\square} / \square g}{}$$

√

□ 1/

2 $c_f k R_s$□$_0$ sin (Z /W_0 2)□

√ (where k = –sin □$_{s0}$) ...(13c)

Note that □$_{s0}$ is the angle of the streamwise vibration direction relative to the tangent to the dam crest, as shown in Figure 3; k is the press shut coefficient, which takes on a negative value for a press-open device (as the skinplate moves downward, the gate opening increases), and a positive value for a press-shut device (as the skinplate moves downward, the gate opening decreases). The symbol c_f represents the instantaneous flow-rate-variation coefficient. In Equations (13), the water head of each pressure fluctuation is divided by a corresponding representative length. The length used for the flow-rate-variation pressure [Equation (13b)] was the magnitude of the change in the gate-opening height. For the push-and-draw pressure [Equation (13a)] and the additional flow-rate-variation pressure [Equation (13c)]), the characteristic length is the streamwise vibration amplitude of the skinplate at its bottom end, since both depend on the skinplate rotation. The amplitudes of □ and □ are represented by □$_0$ and □$_0$, respectively. The radius of the skinplate is represented by R_a. The length R_c is the rotation radius of skinplate lower end about the trunnion pin, as shown in Figure 3. The length R_S is rotation radius of the lower end of the skinplate about its horizontal streamwise-rotation center.

The dimensionless pressure fluctuations defined by Equations (13) can be ultimately reduced to summations of components in phase with the respective velocities and accelerations, as given by the following expressions:

p_r □ p_{rs} □ F/a □ □ p_{rp} □ F/a □^{2} □ ...(14a)

p_b □ □ p_{bs} □ F/a □^{2} □ p_{bp} □ F/a □ □ ...(14b)

p_r □ p_{rs} □ F/a □ □ p_{rp} □ F/a □^{2} □ ...(14c)

In Equation (14b), $\square_p$ is the pressure correction coefficient that accounts for the inclination of the circular-arc skinplate relative to the channel bed. The value of $\square_p$ can be obtained by model experiments, as described in Anami *et al.* (2012b). In the present formulation, the in-air vibration period $1/\square_{a\square}$ of the whole gate vibration around the trunnion pin is adopted as the representative time scale for non-dimensionalizing the time *T*; further, the rotating angular amplitudes $\square_0$ and $\square_0$ are adopted as amplitude scales to reduce vibration amplitudes, respectively:

$t \square \square \square_{a\square} T$; □ □ □ □/ $\square_0$; □ □ □ □/ $\square_0$ ...(15)

F and $F_{a\square}$ represent the Froude number and the basic Froude number, defined by the following expressions:

$F \square \sqrt{\frac{d_0}{g}} \square_w$ and $F_{a\square} \square \sqrt{\frac{d_0}{g}} \square_{a\square}$ ...(16)

which characterize the fluctuating flow field associated with vibrations at circular frequencies of $\square_w$ in water and $\square_{a\square}$ in air. The skinplate submergence depth is represented by d_0.

The dimensionless pressure amplitudes represented by p_{rs}, p_{rp}, p_{bs} and p_{bp} in Equation (14) have been formulated as series summations (Ishii, 1992; and Anami *et al.*, 2012b) as functions of the Froude number *F*, and the reduced height of the streamwise-rotation center, r_s, defined by

$r_s = R_S/d_0$ ...(17)

Subscripts "*s*" and "*p*" on the pressure amplitudes in Equation (14) represent the standing and progressive pressure components, respectively.

Reduced Equations of Motion

Using the non-dimensional parameters introduced in Equation (15), the equation of motion of the whole gate rotational vibration around the trunnion pin, given by Equation (8), can be reduced to the following form:

□ □ □ □ □2□ $_{a\square}$□1
□ □ □□ □ $\square_I$ □ □ □ □ □0 ...(18)
□ □ $\square_*$

where $\square_*$ represents the angular amplitude ratio of the whole gate rotational vibration around the trunnion pin □ to the skinplate streamwise rotational vibration □:

$\square_* \square \square \square_0 / \square_0$ ...(19)

In addition, using the hydrodynamic pressures given by Equations (12) and (13), as well as the non-dimensional variables introduced by Equation (15), the equation of motion for the skinplate streamwise rotational vibration, Equation (11), can be written in the following form:

□
□ □ □ □ □ 2□ $_{a\square}$□ □^{2}□□ $\square_I$□ □ $\square_*$
□□ □□ □ □ □□ $\square_2$ □ □□ □
□□ * □ 1□ y □
0
□ □
□1 p_b□
□ F 2 □1□ r □ dy
a
□ □ s □
□ 1 □0 □ 1□ y

$$[illegible]\; 2\,c_f\,*_r\; F\,2\; [illegible]\; \int_0^1 \frac{1}{a}\,p_r \left(1 - \frac{y}{s}\right) dy \;[illegible]\; 2\,c_f\,k\; F\,2 \int_0^1 \frac{1}{a}\,p_r\, \frac{r}{s}\, dy = 0 \qquad ...(20)$$

where [illegible] represents the in-air natural vibration frequency ratio of the skinplate streamwise rotational vibration [illegible] to the whole gate rotational vibration around the trunnion pin

$$[illegible]\; a\, / \; a \qquad ...(21)$$

Further, $[illegible]_I$ represents the ratio of the coupled moment-of-inertia I to the skinplate moment-of-inertia I, and r_{sa} represents the rotation radius ratio, defined respectively as

$$[illegible]_I = I / I \text{ and } r_{sa} = R_S / R_c \qquad (22)$$

In addition, [illegible] is the mass ratio of the representative water mass to the skinplate mass given by:

$$[illegible] = \frac{[illegible]\, d^2 W_{00}}{I / R_S^2} \qquad ...(23)$$

By substituting the non-dimensional hydrodynamic pressures in the form given by Equations (14) into the equation of motion, Equation (20), one can arrive at the following expression:

$$[illegible]\; 1 \;[illegible]\; m \;[illegible]\; 2\,c\,k \;[illegible]\; m \;[illegible]\; p \;[illegible]\; f \;[illegible]\; 2 \;[illegible]\; a \;[illegible]\; 1 \;[illegible]\; \frac{[illegible]\, c}{2\,c_f\,k\,F} \;[illegible]\; 2 \;[illegible]\; a \;[illegible]\; \frac{m}{[illegible]} \;[illegible]\; \frac{c}{[illegible]} \;[illegible]\; *\;[illegible]\; [illegible]_I \;[illegible]\; 2\,c_f\, r_{sa} \;[illegible]\; 2\,c_f\, r_{sa}\, F_a \;[illegible]\; 2 \qquad ...(24)$$

where $[illegible]_f$ represents the wave-radiation damping ratio, as defined by

$$\zeta_f = \frac{\mu_p \Delta c_\psi}{2 \omega F_a} \quad ...(25)$$

The symbols Δm_ψ and Δc_ψ are the equivalent added mass and the wave-radiation damping coefficient due to the skinplate streamwise rotational vibration, respectively. They are given as

$$\Delta m_\psi = F \int_{1}^{0} \frac{1}{F^2} \left(\frac{1-y}{r_s} \right) p_{bs}\, dy \quad ...(26a)$$

$$\Delta c_\psi = F \int_{1}^{0} \frac{1}{F} \left(\frac{1-y}{r_s} \right) p_{bp}\, dy \quad ...(26b)$$

The symbols Δm_θ and Δc_θ are the equivalent added mass and the fluid-excitation coefficient due to the whole gate rotational vibration, respectively. They are given as

$$\Delta m_\theta = \frac{1}{2F^2} \int_{1}^{0} \left(\frac{1-y}{r_s} \right) p_{rp}\, dy \quad ...(27a)$$

$$\Delta c_\theta = \frac{1}{2F} \int_{1}^{0} \left(\frac{1-y}{r_s} \right) p_{rs}\, dy \quad ...(27b)$$

In Equation (24), the equation of motion for the skinplate streamwise rotational vibration, the second term on the right-hand side, the one proportional to velocity, is most significant for stability. This term results from the flow-rate variation and drives the coupled-mode self-excited vibration. The parameter ζ_f in the second term on the left-hand side represents the wave-radiation damping effect due to dissipative waves and is dependant upon the dissipative wave-radiation damping coefficient Δc_ψ. As the Froude number increases, the dissipative wave-radiation damping coefficient Δc_ψ decreases rapidly and takes on an almost zero value for large Froude number. The parameter $\mu_\psi \Delta m_\psi$ in the first term on the left-hand side represents the added mass effect of the fluid, which significantly reduces the in-air natural vibration frequency when the gate vibrates in water.

The calculated values for the flow-induced factors Δm_θ, Δc_θ, Δm_ψ, and Δc_ψ are shown in Figure 4. All of these flow-induced factors are functions of the Froude number. As the Froude number increases, the reduced added mass

Δm_θ decreases rapidly and is nearly zero for Froude numbers F larger than about 2. As a result, the reduced added mass effect due to the whole gate rotational vibration around the trunnion pin has no effect on neither the whole gate vibration nor on the skinplate streamwise rotational vibration. When the Froude number F is larger than about 10, the dissipative wave-radiation damping coefficient Δc_ψ also approaches zero. In contrast, the fluid excitation coefficient Δc_θ increases rapidly from zero and asymptotically approaches a comparatively large value, signifying a comparatively large fluid-excitation effect for sufficiently large Froude numbers. This is the significant factor which drives the self-excited vibration of the coupled-mode vibration system. In addition, the reduced added mass Δm_ψ also increases rapidly from zero, and approaches an asymptotic value at large Froude numbers resulting in a significant frequency reduction for the streamwise rotational vibration relative to its in-air value.

The equation of motion, Equation (24), for the skinplate streamwise rotational vibration when arranged in standard form with the coefficient of □" equal to 1.0 becomes:

□ 2 □□ □c□
□
□ a □ f □ c k
□ □ □ f F □
a □
□ □ □ □ □ □ □ □
2□□ □ □
1□ 2
□ □ □m □ 2 c k□ □m
p □ □ √ f □ □
□

□□ □
2 √
□ □
1□ 2
□ □ □m □ 2 c k□ □m
p □□ √ f □ □
□

□□
□□ □m□ □ □□ □c□
□ □
□□ □ □ □ □ □
□□2 □I□ □ 2 c_f r 2 c_f r F □
□ □ □ sa □ sa a□
□*
□ □□ 2
1 □ □ □m □ 2 c k□ □m
p
□ □ √ f □ □
□

...(28)

Int. J. Mech. Eng. & Rob. Res. 2014 ***Keiko Anami et al., 2014***

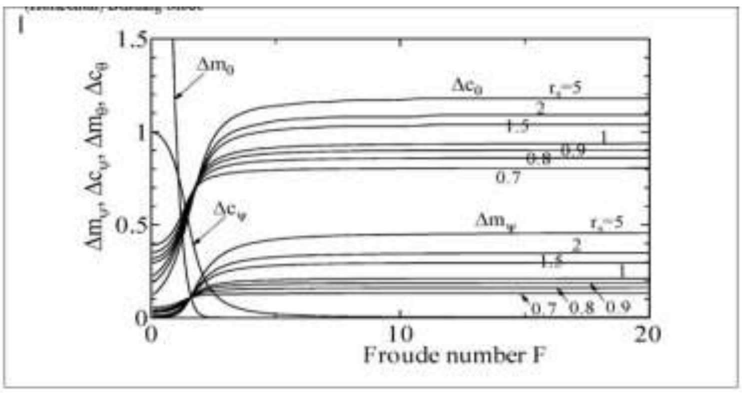

Figure 4: Equivalent Added Mass Coefficients, □m□ and □m□, Wave-Radiation Damping Coefficient, □c□ and Fluid-Excitation Coefficient, □c□, for kinplate Vibration in the 1/2 Wave-Length Transverse (Horizontal) Bending Mode

The coefficient of □ gives the in-water to in-air vibration frequency ratio $□_{nw}$ in the following form:

□ □*nw* □ □□
□ □
□□ □ □□
nw
□ □
□*a*□
□ □ 1□ □ □ □ □*m*2
□ 2 *c* *k*□ □*m*
p □ □ *f* □ □
□

...(29)

The denominator $□_{a□}$ represents the in-air vibration frequency of the whole gate rotational vibration around the trunnion pin, which takes on essentially the same value as the in-water

□ *nw* □ □ *nw*□ □□ □ ...(30)

where $□_{nw□}$ is the in-water to in-air vibration frequency ratio of the skinplate streamwise vibration:

□ □*nw*□ □ 1
□□ □ □□
nw
□ □ □
□ □*a*□ □ 1□ $□_p$□ □*m*□2
□ 2 c_f *k*□ □*m*□
□

...(31) With these vibration frequency ratios, the equation of motion for the skinplate, Equation

(28), can be ultimately arranged as follows:

natural vibration frequency, since no added mass effect arises due to the whole gate vibration around the trunnion pin.

Using the in-air vibration frequency ratio □□□ □ □ □ □*a*□ / $□_{a□}$ □ defined by Equation (22), $□_{nw}$
This is the final form of the equation of motion of the skinplate streamwise vibration.

Approximate Solution

The coupled-mode vibration system involves two natural vibration frequencies, one for the whole gate rotational vibration around the trunnion pin, and one for the skinplate streamwise rotational vibration. The coupled-mode vibration occurs, in essence, when the two frequencies coalesce. The resulting synchronized vibration occurs with one of the natural vibration modes serving as the driving excitation for the other mode. Through the feedback of one mode driving the other, the coupled-mode self-excited vibration is built up. In the following, the driving vibration will be called the “main vibration”, and the other mode that responds to the forcing of the first mode will be called the “response vibration” or the “dependent vibration”. With this understanding of the physical situation, the equations of motion, Equations (18) and (32), for coupled-mode vibration can be solved approximately.

Whole Gate Mode Synchronized with Skinplate Streamwise Vibration

First, assume the following periodic solution for the main vibration, that is, for the skinplate streamwise rotational vibration:

□ □ cos □ *t* ...(33)

□ is the frequency ratio of the in-water streamwise rotational vibration $□_{w□}$ to the representative in-air vibration $□_{a□}$:

$$□ □ □ □_{w□} / □_{a□} \quad ...(34)$$

With this frequency, the Froude number F is given by

$$F □ \sqrt{\frac{d_0}{g}} □_{w□} □ F_{a□} □ \quad ...(35)$$

Therefore, the equation of motion, Equation (18), of the whole gate rotational vibration around the trunnion pin (response vibration) is expressed as follows:

$$□□ □ □ □ \quad 2□\frac{1}{□ □ □_*} \quad {}_{a□}□□ □ □□ □ \quad □_I □^2 \cos □ t \quad ...(36)$$

This is the equation of motion of the so-called forced vibration (response vibration) with the cos□ t term on the right-hand side. This forced vibration has a solution in the following form:

$$□ □ \cos □□ t □ □ □ \quad ...(37)$$

The problem can be reduced to one of calculating the angular-amplitude ratio $□_*$ and phase-lag□ from the two expressions, Equations (36) and (37). Substituting Equation (37) into the equation of motion for the whole gate as a rigid-body, Equation (36), one can arrive at the following equation:

$$\sqrt{□1□ □^2 □^2 □ □2□ □_{a□} □^2} \cos □□ t □ □ □ □_□ \frac{1}{□ □ □_*} □_I □^2 \cos □ t \quad ...(38)$$

where $□_□$ is given by

$$□_□ \quad \tan \frac{□1}{□2□ □a□} \quad 1□ 2 □ \quad ...(39)$$

As a result, the following solutions $□_*$ and □ can be derived:

$$□_*□ □□ \quad \frac{1}{□} \frac{□_I□ □ □^2}{\sqrt{□1□ □^2 □^2 □ □2□ □_{a□} □^2}} \quad ...(40)$$

$$□ □ □ □_□ □ □□ \quad \tan \frac{□1}{2□ □a} \quad 1□ 2 □ \quad ...(41)$$

Since the responding whole gate rotational vibration □ was obtained for the assumed streamwise rotational vibration □, the feedback process of the above solution to the main skinplate streamwise vibration must be analyzed. Upon substitution of Equation (37) into the equation of motion for the skinplate streamwise rotational vibration (the main vibration), Equation (32), the following equation of self-excited vibration can be derived:

□1□ □ $_{nw}^{2}$□ □m□ □ □□ □ □

□ □□ □c□ □
□ 2 □c□ □ □
□ 2□ nw □□ □ □□ √ □
nw□ □ a□ □$_f$□ □ $c_f\, k$ □ □
$^F a$□ □ □ □ □
□ □ □□ □□
□ □ ^{2} □ □ 0 ...(42)
nw

where □m□ □ and □c□ □ are the reduced added mass coefficient and reduced fluid-excitation coefficient due to the coupling of two vibration modes:

where □$_f$□ is the fluid-excitation ratio, defined by

□$_f$ □c□ □ □ □□□$_f$ √2 □c□
□ □ □□ □ □ $c_f\, k$ $^F a$□ ...(46)
□□ □ □ □□

The square root of the coefficient on □ in Equation (45) represents the actual frequency ratio □$_w$□ □ of the in-water skinplate streamwise rotational vibration to the whole gate in-air vibration frequency:

□$_w$□
□ □□ □ nw
□□ □ □ □
w□
□ □ □ √
□a□
□ □ 1 □ □ $_{nw}^{2}$ □ Δm□ □
□
√ □
□
√
1 □ 2
□ □ Δm □ 2 c k□ Δm □ Δm
□
√ p □ □ √ f □ □ □
□
√
...(47)

If the actual frequency ratio □$_w$□ □ obtained here is not in agreement with the frequency ratio □ of Equation (34) assumed first, □$_w$□ □ is replaced by □, and the ultimate solutions of the vibration ratio □$_w$□ □ can be obtained by iterative calculations of Equations (40), (41), (43), and (47). Using the solution for the frequency ratio, the equation of motion, Equation (45), can be reduced to:

□ □□$_w^2$ □□ $_a$□ □ □$_f$□ □□ □ □ □ □
□ □ □ □□ $_w^2$□ □□ □ 0 ...(48)

2
□□ □

From the coefficient on □', the actual excitation ratio □□ of the skinplate streamwise rotational vibration (main vibration) can be given by:

□w□
□ □
□ □ □□f□□ □ □ □□a□□ □...(49)
□□ □

Subsequently, Equation (42) can be arranged as follows:

□ a□ □□ □
□ □ □ □ □f□ □ □ □ □nw² □ □
2□□□ 1□ □² □m □ 1□ □² □m 0
nw □ nw
□ □ □ □ □

...(45)

Skinplate Streamwise Vibration Synchronized with Whole Gate Rotational Vibration

Here, assume the following periodic solution for the whole gate rotational vibration around the trunnion pin:

□ □ cos □ t ...(50)

where □ is the frequency ratio of in-water rotational vibration around the trunnion pin □w□ to the representative in- air vibration □a□:

□ □ □ □w□ / □a□ ...(51)

Using the in-water vibration frequency □w□, the Froude number F is given by

F □ $\sqrt{d_0 / g}$ □w□ □F a□ □ ...(52)

Using Equation (50), the right-hand side of the equation of motion, Equation (32), for the skinplate streamwise vibration can be arranged as follows:

Right-hand-side Substituting Equation (53) into the right-hand side of the equation of motion, Equation (32), the following equation of motion for the forced vibration (the response vibration) can be obtained:

□ 2 □c□ □
□ □
□ □ □ □ □2□ nw□ □□ a□ □ □ □
nw □ f□ □ c_f k F a□ □
□ □ □□ □ □
□ □² □ □ □cos □□t □
f □ □ ...(56)
*
nw □ 0

The solution of this forced vibration can be assumed to be of the following form:

□ □ cos □□ t □ □0 □ □
□ ...(57)

where the angular-amplitude ratio □* and phase-lag □ are given by [illegible] $\ldots$ $2\,nw\,nw$ $\ldots$ a $\ldots$ $c_f\,k$ $\ldots$ F $\ldots$ a [illegible]

...(58)

[illegible] $\tan$ $\ldots$ $n\,nw$ $\ldots$ a $\ldots$ f $\ldots$ $c_f\,k$ $\ldots$ $F\,a$ $\ldots$ $2\,n_w$ [illegible]

...(59)

Since the responding skinplate streamwise vibration [illegible] was obtained for the main whole gate vibration [illegible], it is necessary to analyze the feedback process to the main whole gate vibration. Representing [illegible]” in the equation of motion, Equation (18), of the main whole gate vibration in terms of [illegible] ” and [illegible] ’, respectively, the following equation of motion for the self-excited vibration system can be derived:

[illegible] $\frac{1}{\ast}$ $\ldots$ $\cos$ $\ldots_0$ $\ldots$ $\sin$ $\ldots$ $2\ldots_a$ $\ldots = 0$ [illegible]

...(60)

which can be reduced ultimately to the following expression:

[illegible] $1 \ldots m \ldots 2 \ldots_a \ldots c \ldots = 0$ [illegible]

...(61)

where [illegible] m and [illegible] c are the reduced added mass and the reduced dissipative wave-radiation damping coefficient due to the coupling of two vibration modes:

[illegible] $m = \frac{1}{\ast} \ldots \cos \ldots_0 \ldots$ [illegible]

...(62)

[illegible] $c = \frac{1}{2 \ast} \ldots \sin \ldots_0 \ldots$ [illegible]

...(63)

Therefore, the equation of motion, Equation (61), can be arranged as follows:

[illegible] a $\ldots$ f $\ldots 1 \ldots = 0$ [illegible]

...(64)

□2 □

1□ □ □*m*□ □ 1□ □ □*m*□ □

where □$_{f□}$ is the fluid-excitation ratio:

□$_{f□}$ □ □ □*c*□ □ ...(65)

The square root of the coefficient of □ in Equation (64) gives the in-water to in-air vibration frequency ratio □$_{w□ □}$ for the whole gate rotation around the trunnion pin:

□ □*w* □

□ 1

□□ □ □ □

w□

□

□ □ ...(66)

□*a*□ √

□ □ 1□ □ □*m*□ □

If this frequency ratio □$_{w□ □}$ is not in agreement with the frequency ratio □ which was first assumed in Equation (51), □$_{w□ □}$ is replaced by □, and the ultimate solution of the vibration ratio □$_{w□ □}$ can be obtained by iterative calculations of Equations (58), (59), (62), and (66). Using the solution of frequency ratio, the equation of motion, Equation (64), can be expressed in the following form:

□ □ □ □ □2□$_w^2$□ □ □□ $_{a□}$ □ □$_{f□}$ □□

□ □ □□$_w^2$□ □□ □ 0 ...(67)

From the coefficient on □', the actual excitation ratio □□ of the whole gate rotational vibration (main vibration) can be obtained as follows:

□□□ □□□ □ □$_{w□ □}$□□□$_{f□}$□□□ □

□$_{a□}$□□ ...(68)

Finally, the dynamic stability criteria can be given by the following conditions that force the actual excitation ratio □□ and □□ to be negative:

□$_{a□}$>□$_{f□}$ (when synchronized with the

skinplate streamwise vibration) ...(69)

□$_{a□}$>□$_{f□}$ (when synchronized with the whole

gate rotational vibration) ...(70)

where □$_{a□}$ and □$_{a□}$ are the damping ratios necessary for the skinplate streamwise vibration and for the whole gate rotation to be dynamically stable, respectively.

Characteristics of Coupled-Mode Self-Excited Vibration

The approximate solutions are calculated specifically for the case of Folsom Dam Tainter gate. The major specifications of Folsom Tainter gate at the time of failure are shown in Table 1. The average gate opening B was 0.762 m, 5.7% of the water depth d_0 of 13.26 m, and hence it can be treated as a small gate opening. The moment of inertia of the gate was calculated from the mass and dimensions of each component. The spanwise (i.e., horizontal) nodal line of the skinplate, that is, the skinplate streamwise rotation center height R_S was 9.6 m. Values of the following parameters were obtained from the experimental modal analyses on a

Figure 6: Vibration Trajectory Formation and Energy Supply, When Synchronized with the Streamwise Rotational Vibration of Circular-Arc Skinplate: (a) Vibration Trajectory at □$_{nw}$<1.0; (b) Exciting Forces: ①

Coupled inertia force; ② Flow-Rate Variation Fluid Force; (c) Energy Supply by Resultant Force to Streamwise Vibration, at $\square_{nw}$<1.0;

(d) Vibration Trajectory at $\square_{nw}$>1.0; (e) Energy Supply by Resultant Force to Streamwise Vibration, at $\square_{nw}$>1.0

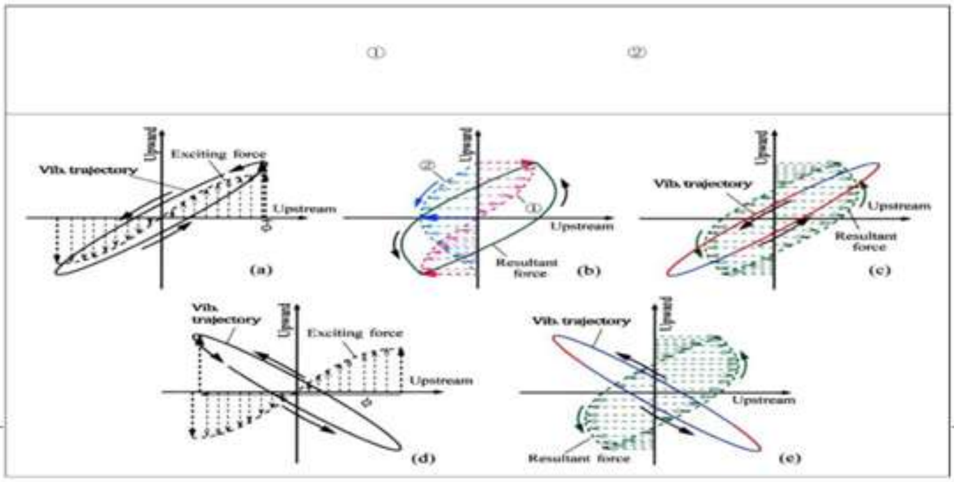

This exciting force would then appear in the opposite direction when the skinplate moves upward. Figure 6c shows both the vibration trajectory and the resultant excitation force. The red lines of the vibration trajectory show when the resultant excitation force supplies energy to the streamwise vibration, while the blue lines show when the vibration energy is consumed. As is clear from Figure 6c, the supplied energy is far larger than the consumed energy, thus inducing the intense dynamic instability observed for point "q" in Figure 5b.

When the natural vibration frequency ratio is in $\square_{nw}$>1.0, the phase-lag takes on a value from 90° to 180°. Since the damping ratio of the whole gate rotational vibration around the trunnion pin is quite small, the phase-lag takes on a large value near 180°. Then, when the skinplate comes to its most downstream position, the maximum upward vibration response appears, as shown in Figure 6d. As a result, the vibration trajectory in this case shows a thin press-open trajectory. The trajectory has a counter-clockwise rotation.

Figure 6e shows both the press-open trajectory and the resultant excitation force. The energy consumption region, shown by the blue lines, is far larger than the energy supply shown by the red. As a result, when the trajectory corresponds to a press-open device, the system exhibits strong dynamic stability with no chance of coupled-mode vibration, as in point "u" in Figure 5b.

Coupled-Mode Vibration Synchronized with the Whole Gate Rotational Vibration

When the whole gate performs rotational vibration around the trunnion pin, the coupled inertia torque of the skinplate and the torque due to the flow-rate variation pressure are induced, thus forcing the circular-arc skinplate to vibrate in the streamwise direction. These torques appear on the right-hand side of equation of motion, Equation (32). The streamwise resultant exciting force due to these torques is illustrated in Figure 6b and again by the dashed line in Figure 7a. The maximum exciting force in the downstream direction appears with a phase-lag between 90° and 180° from the most upward position of the skinplate. This streamwise exciting force induces the maximum vibration response in the downstream direction, however with a phase-lag which is determined by Equation (32).

When the natural vibration frequency ratio $\square_{nw}$<1.0, that is, when the natural vibration frequency $\square_{a\square}$ of the main vibration is higher than the natural vibration frequency $\square_{nw\square}$ of the response vibration, the downstream maximum vibration response appears with a phase-lag of about 180°, as shown by the arrows along the vertical axis in Figure 7a. As a result, the vibration trajectory shows a thick press-open characteristic, as illustrated by the solid line in Figure 7a. The trajectory has a clockwise rotation.

vibration. The coupled inertia torque of the right-hand side of the equation of motion, Equation (18), induces the up-and-down vibration of the skinplate. The upward inertia force becomes largest when the skinplate reaches its most upstream position, as shown in Figure 6a and again by the dotted line in Figure 7b. The energy supply lines shown in red are far smaller than the energy consumption lines shown in blue. Thus, the system is dynamically stable, as shown by point "t" in Figure 5b.

When the natural vibration frequency ratio $\square_{nw}$>1.0, that is, when the natural vibration frequency $\square_{a\square}$ of the main vibration is lower than the natural vibration frequency $\square_{nw\square}$ of the response vibration, the downstream maximum vibration response appears with a phase-lag of almost 0°, as shown by small arrows along the vertical axis in Figure 7c. As a result, the vibration trajectory shows a thick press-open characteristic, as illustrated in Figure 7c. The trajectory shows a counter-clockwise rotation.

Figure 7d shows both of the vibration trajectory and the resultant excitation force, where the energy supply region shown in red is far larger than the energy consumption region shown in blue. Thus, the vibration results in the dynamic instability shown by point "r" shown in Figure 5b.

Instability of the Folsom Gate for Conditions at Failure

The fluid-excitation ratios for the Folsom Dam Tainter gate under its failure conditions were theoretically calculated, as shown in Figure 5b. The ordinate represents the damping ratio needed to prevent the dynamic instability, that is, so-called the "stability damping ratio".

Figure 7: Vibration Trajectory Formation and Energy Supply, When Synchronized with the Whole Gate Rotational Vibration Around Trunnion Pin: (a) Vibration Trajectory at $\square_{nw}$<1.0; (b) Energy Supply by Inertial Force to Up- and Downward Vibration, at $\square_{nw}$<1.0;

(c) Vibration Trajectory at $\square_{nw}$>1.0; (d) Energy Supply by Inertial Force to Up- and Downward Vibration, at $\square_{nw}$>1.0

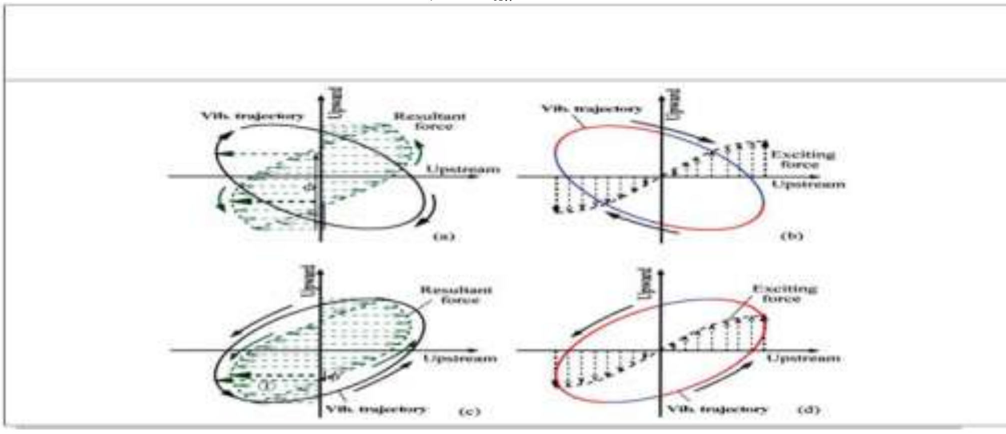

Therefore, by using this calculated result and the measured vibration characteristics (vibration frequencies, damping ratios) of the Folsom Dam Tainter gate, its dynamic stability at failure can be discussed.

The in-air streamwise natural vibration frequency $\square_{a\square}$ of the skinplate of Folsom Dam Tainter gate takes on a value of 26.9 Hz from field testing of the experimental modal analysis by Ishii (1995a and 1995b), Anami *et al.* (2014), but is drastically decreased by the added mass effect of the water, as described in Anami and Ishii (1998b) and Anami *et al.* (2012b). The in-water to in-air vibration frequency ratio $\square_{nw\square}/\square_{a\square}$ of the skinplate streamwise rotational vibration can be calculated from Equation (31). Introducing the inherent Froude number $\square_{nw\square}$ and the basic Froude number $\square_{a\square}$ for streamwise vibration of the skinplate, defined by

Figure 8: In-Water to In-Air Vibration Frequency Ratio for Folsom Dam Tainter Gate

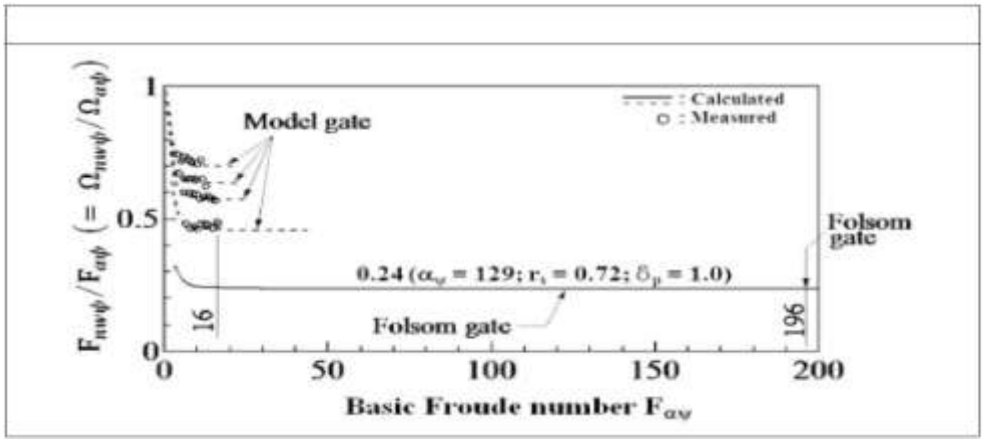

1

□

) 2

1□ □ □ □□m (F □ 2 c k□ □m (F)

nw nw

p □ □ □ √ f □ □ □

□

...(75)

The reduced water added mass □m□ and □m□ on the right hand side of Equation (75) are functions of the inherent Froude number $F_{nw□}$ and the reduced rotation center height r_s; their characteristic behavior is shown in Figure 4. Therefore, computer calculations can be performed to determine the inherent Froude number $F_{nw□}$ for a given value of the basic Froude number $F_{a□}$. The calculated results can be reduced to $F_{nw□}/F_{a□}$, which represents the in-water to in-air vibration frequency ratio $□_{nw□}/ □_{a□}$, as shown by the solid line in Figure 8. In this figure theoretical values for both the Folsom gate and the model gate are shown as solid and dashed lines, respectively. Experimental values for the model gate are shown as well, providing evidence of the applicability of the theoretical results. For the Folsom Dam Tainter gate, the following values were used in the calculations: the reduced rotation center height r_s was 0.72; the water-to-gate mass ratio □□ was 129; and the pressure correction coefficient $□_p$ was 1.0. From Figure 8, the in-water to in-air vibration frequency ratio $□_{nw□}/□_{a□}$ takes a constant value of 0.24 for basic Froude number $F_{a□}$ values greater than about 20. The present calculated results are esentially identical to Figure 3b in a study by Anami *et al.* (2012b), in which the single mode of streamwise vibration of the skinplate was considered.

With the measured in-air natural vibration frequency $□_{a□□}$ of 26.9 Hz and the gate submergence depth d_0 of 13.26 m for the Folsom Dam Tainter gate at its failure, the basic Froude number $F_{a□}$ takes a large value of 196. Therefore, the in-water to in-air vibration frequency ratio $□_{nw□}/□_{a□}$ takes on a value of 0.24, which is far smaller than that for the model test results (see Anami *et al.*,

Figure 9: Dynamic Instability for the Failed Tainter Gate at the Folsom Dam

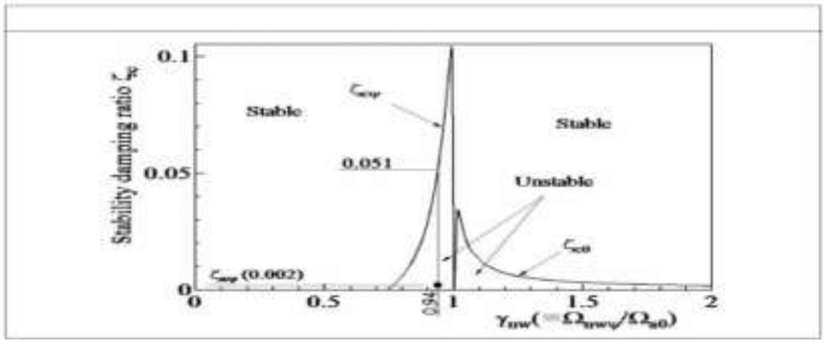

2012b), shown by dashed lines in Figure 8. This is because the Folsom Tainter gate has a water-to-gate mass ratio □□ of 129, far larger than the value of 2.45 to 14.8 for model gate testing. The ratio of 0.24 for Folsom Dam gate means the in-water vibration frequency was slightly less than ¼ of the measured in-air natural vibration frequency $□_{a□}$ of 26.9 Hz, or more precisely 6.46 Hz. It is important to note here that the frequency of streamwise bending is just slightly smaller than the in-air natural vibration frequency $□_{a□}$ of 6.88 Hz for the whole gate vibration around the trunnion pin. The resulting frequency ratio $□_{nw}(=□_{nw□}/ □_{a□})$ takes on a value of 0.94, just slightly smaller than 0.96 at which the maximum instability occurs. The measured in-air damping ratio $□_{a□}$ of 0.002 of the skinplate streamwise vibration is plotted on the stability curve in Figure 9. For this mode of vibration, with nodes along the sides of the gate, the damping due to the side seals plays no role in the streamwise bending vibration. The difference between the fluid dynamic excitation ratio and the existing structural damping ratio is about 0.049, indicating an additional 5% damping would be needed to stabilize the gate. Increases in damping due to water have been included in the theory. As a result, one may conclude that the dynamic condition of the Folsom Dam Tainter gate under the prevailing conditions at the moment of failure was situated in the intense dynamic instability region. This dynamic condition indicates the gate was readily susceptible to coupled-mode vibration, which would induce a violent coupled-mode vibration synchronized with the skinplate streamwise rotational bending vibration, which would serve as the main vibration at the incipient failure.

III. CONCLUSION

Based on experimentally determined dynamic characteristics for the Folsom Dam Tainter gate and using previously derived and validated expressions for pressure loading and added mass effects, equations of motion were derived for the two predominant vibration modes believed to have played a role in the Folsom gate failure. An approximate, iterative method of solution was employed to solve the two coupled equations. From the solutions, dynamic stability diagrams were derived.

The resulting solution demonstrates the existence of two regions of instability, one in which the frequency of the skinplate bending mode is just slightly less than the natural frequency of the rigid-body mode. In this region the skinplate bending acts as the main driving force and the rigid body rotation is the response mode. This is the most unstable situation. The second region of instability occurs when the frequency of the skinplate bending mode is just slightly higher than that of the rigid body rotation. In this region the rigid-body motion is the driving force and the bending mode is the response vibration. In this region, instability is still evident, but its intensity is reduced relative to that of the first region.

On the basis of this analysis, the Folsom Dam was shown to possess a strong dynamic instability for the conditions that pertained at the instant of gate failure. There is every reason to believe that this coupled-mode self-excited instability could well have played a very strong (if not dominant) role in the failure of the Folsom gate.

More importantly, the theory provides an assessment tool to determine the susceptibility of any Tainter gate to this coupled-mode self- excited instability. The necessary inputs are the gate and sill geometry (from the drawings for the installation), the expected range of depth of the upstream reservoir, the skinplate in-air natural vibration characteristics (frequency, mode shape and damping ratio, usually from experimental modal analysis) for the lowest frequency bending mode of the skinplate, and the rigid-body rotational frequency and damping ratio.

ACKNOWLEDGMENT

Financial support was provided by a Grant-in-Aid for Science Research of Japan Society for the Promotion of Science.

REFERENCES

[1]. Anami K and Ishii N (1998a), "In-Water Streamwise Vibration of Folsom Dam Radial Gates in California", Proceedings of 1998 ASME Pressure Vessels and Piping Conf., Vol. 363, pp. 87-93.

[2]. Anami K and Ishii N (1998b), "In-Air and In-Water Natural Vibrations of Folsom Dam Radial Gate in California", Proceedings of 11th International Conference on Experimental Mechanics, Experimental Mechanics 1, in Allison (Ed.), pp. 29-34, Rotterdam, Balkema.

[3]. Anami K, Ishii N and Knisely C W (2012a), "Pressure Induced by Vertical Planar and Inclined Curved Weir Plates Undergoing Streamwise Rotational Vibration", *J. Fluids and Structures*, Vol. 29, pp. 35-49.

[4]. Anami K, Ishii N and Knisely C W (2012b), "Added Mass and Wave Radiation Damping for Flow-Induced Rotational Vibrations of Skinplate", *J. Fluids and Structures*, Vol. 35, pp. 213-228.

[5]. Anami K, Ishii N and Knisely C W (2014), "Retrospective Considerations of Vibration Mechanism for Folsom Dam Tainter Gate Failure", *Intern. J. Mech. Engineering and Robotics Research*, Vol. 3, No. 4.

[6]. Imaichi K and Ishii N (1977), "Instability of an Idealized Tainter Gate System Without Damping Caused by Surface Waves on the Backwater of Dam", *Bulletin of the Japan Society of Mechanical Engineers*, Vol. 20, No. 146, pp. 963-970.

[7]. Ishii N (1992), "Flow-Induced Vibration of Long-Span Gates (Part I: Model Development)", *J. Fluids and Structures*, Vol. 6, pp. 539-562.

[8]. Ishii N (1995a), "Folsom Dam Gate Failure Evaluation and Suggestions", Report Submitted to US Bureau of Reclamation, August 24.

[9]. Ishii N (1995b), "Folsom Dam Gate Failure Evaluation Based on Modal Analysis and Suggestion", Report Submitted to US Bureau of Reclamation, November 8.

[10]. Ishii N (1997), "Dynamic Stability Evaluation for Folsom Dam Radial Gate and its Inherent Non-Eccentricity Instability", Report Submitted to US Bureau of Reclamation, July 17.

[11]. Ishii N and Imaichi K (1977), "Water Waves and Structural Loads Caused by a Periodic Change of Discharge from a Sluice Gates", *Bulletin of the Japan Society of Mechanical Engineers*, Vol. 20, No. 6, pp. 998-1007.

[12]. Ishii N, Imaichi K and Hirose A (1977), "Instability of Elasticity Suspended Tainter Gate System Caused by Surface Waves on the Upstream Channel of a Dam",
[13]. *ASME Journal of Fluids Engineering*, Vol. 99-4, pp. 699-708.
[14]. Ishii N, Imaichi K and Hirose A (1979), "Dynamic Instability of Tainter Gates",
[15]. *Practical Experiences with Flow-Induced Vibrations*, in E Naudascher and D O Rockwell (Eds.), pp. 452-460, Springer, Berlin.
[16]. Ishii N and Naudascher E (1992), "A Design Criterion for Dynamic Stability of Tainter Gates", *J. Fluids and Structures*, Vol. 6, pp. 67-84.
[17]. Rayleigh J W S (1945), *The Theory of Sound*, Vol. 2, pp. 4-8, Dover, New York.

APPENDIX

Nomenclature

B:	discharge gate opening
c_f:	instantaneous flow-rate variation coefficient
d_0:	skinplate submergence depth
$dM_{□□}$, $dM_{□□}$:	coupled moment
F:	Froude number
$^{F}a□$, $^{F}a□$:	basic Froude number
$^{F}nw□$:	inherent Froude number
g:	acceleration due to gravity
$I_{□}$:	moment-of-inertia of whole gate rotation around trunnion pin
$I_{□}$:	moment-of-inertia of skinplate streamwise rotation
$I_{□□}$:	coupled moment-of-inertia
k:	press-shut coefficient
P, $P_{b□}$, $P_{r□}$, $P_{r□}$:	hydraulic pressure
$^{p}b□$, $^{p}r□$, $^{p}r□$:	reduced hydrodynamic pressure
p_{bs}, p_{rs}:	amplitude of standing pressure wave component
p_{bp}, p_{rp}:	amplitude of progressive pressure wave component
R_a:	length of radial arm
R_c:	rotation radius of skinplate lower end
R_S, r_s:	rotation center height
r_{sa}:	ratio of rotation radius
$R_{□}$:	distance from skinplate rotation center to skinplate small area
T, t:	time
W_0:	spanwise length
X:	coordinate along undisturbed free surface toward upstream side
Y:	upward coordinate along skinplate
Z:	horizontal coordinate along skinplate from its center
$□_*$:	vibration angular amplitude ratio
$□_I$, $□_{I□}$:	ratio of moment of inertia
$□_{□}$:	water-to-skinplate mass ratio
□*:	depth ratio

□$_{nw}$:	ratio of in-water natural frequencies of coupled-mode vibration
□nw□:	in-air to in-water natural frequency ratio of streamwise vibration
□w□ □:	in-air to in-water natural frequency ratio of whole gate rotational vibration around trunnion pin
□w□□:	actual vibration frequency ratio of streamwise vibration to in-air rotational vibration around trunnion pin
□$_{□□}$:	in-air vibration frequency ratio

APPENDIX (CONT.)

□$c_{□□}$:	reduced fluid excitation coefficient due to coupling
□$c_{□□}$:	reduced wave-radiation damping coefficient due to coupling
□$C_□$, □$c_□$:	wave-radiation damping coefficient
□$I_□$:	corrected moment of inertia
□$m_□$, □$m_□$:	reduced added mass
□$m_{□□}$, □$m_{□□}$:	reduced added mass due to coupling
□$_p$:	pressure correction coefficient
□$_a$:	in-air damping ratio (without coupling)
□$_{a□}$:	in-air damping ratio of rotational vibration around trunnion pin
□$_{a□}$:	in-air damping ratio of streamwise rotational vibration
□$_f$, □$_{f□}$:	wave-radiation damping ratio
□$_w$:	in-water streamwise damping ratio (without coupling)
□ □ □□:	counter-clockwise rotation angle of whole gate rotation around trunnion pin
□$_0$, □$_0$:	amplitude of □ and □
□$_{ps}$:	press-shut angle of vibration trajectory
□$_{s0}$:	geometric press-open angle
□$_{f□}$, □$_{f□}$:	fluid excitation ratio
□$_□$, □$_□$:	actual excitation ratio
□,□:	counter-clockwise rotation angle of skinplate streamwise vibration

□$_a$:in-air natural vibration frequency ratio (without coupling) [rad/s]

□$_{a□}$:in-air natural vibration frequency of whole gate rotation around trunnion pin

□$_{a□}$: in-air streamwise natural vibration frequency ratio [rad/s]

□$_w$:in-water vibration frequency ratio (without coupling) [rad/s]

□$_{w□}$:in-water vibration frequency of rotational vibration around trunnion pin [rad/s]

□$_{nw□}$:in-water streamwise natural vibration frequency [rad/s]

□$_{w□}$:in-water streamwise vibration frequency [rad/s]

Subcripts

$(\ )_a$	in-air
$(\ )_w$	in-water

( )□ related to the rigid body rotation around the trunnion pin

( )□ related to the skinplate bending mode